LAWRENCE
LIVERMORE
NATIONAL
LABORATORY

LLNL-CONF-432609

# Streaked radiography measurements of convergent ablator performance

D. G. Hicks, B. K. Spears, D. G. Braun, R. E. Olson, C. M. Sorce, P. M. Celliers, G. W. Collins, O. L. Landen

May 18, 2010

Measuring implosion performance using streaked radiography
Wildwood, NJ, United States
May 17, 2010 through May 20, 2010

## Disclaimer

# Streaked radiography measurements of convergent ablator performance[a)]

D. G. Hicks,[1, b)] B. K. Spears,[1] D. G. Braun,[1] R. E. Olson,[2] C. M. Sorce,[1] P. M. Celliers,[1] G. W. Collins,[1] and O. L. Landen[1]

[1)] *Lawrence Livermore National Laboratory, Livermore, CA 94550*

[2)] *Sandia National Laboratory, Albuquerque, New Mexico 87185*

(Dated: 17 June 2010)

The velocity and remaining ablator mass of an imploding capsule are critical metrics for assessing the progress towards ignition of an inertially confined fusion experiment. These and other ablator rocket parameters have been measured using a single streaked x-ray radiograph. A regularization technique has been used to determine the ablator density profile, $\rho(r)$, at each time step; moments of $\rho(r)$ then provide the areal density, average radius, and mass of the unablated, or remaining, ablator material, with the velocity determined from the time derivative of the average radius. The technique has been implemented on experiments at the OMEGA laser facility.

[a)]Invited paper, published as part of the Proceedings of the 18th Topical Conference on High-Temperature Plasma Diagnostics, Wildwood, New Jersey, USA, May 2010.

[b)]Author to whom correspondence should be addressed. Electronic mail: hicks13@llnl.gov.

## I. INTRODUCTION

The experimental plan for achieving indirectly-driven ignition at the National Ignition Facility[1] (NIF) requires the measurement and tuning of several key metrics each of which characterize different aspects of the implosion[2]. These metrics include the x-ray conversion efficiency, implosion symmetry, fuel adiabat, and fuel velocity. High fuel velocities are required to deliver compressive energy to the hot spot faster than it is lost via conduction or radiation and is one of the most important figures-of-merit in Inertial Confinement Fusion. Calculations show that the ignition threshold scales as the inverse sixth power of the velocity[3–5].

Achieving a high fuel velocity involves a balance between two competing requirements[6]: (1) Burning off most of the ablator mass to minimize the rocket payload, and (2) Preserving sufficient ablator mass to keep ablator-fuel interface instabilities and fuel pre-heat effects low. The maximum velocity desired is that which can be achieved with sufficiently low mix and pre-heat of the fuel. For typical indirectly-driven NIF ignition targets, radiation-hydrodynamic simulations have established that the optimal peak velocity is in the range 350-380 $\mu$m/ns while the remaining mass of the ablator is 5-15% of the initial ablator mass. The precise values depend sensitively upon the mix and transport models used in the simulations as well as on specifics of the target and laser drive.

For a given laser drive and target configuration, whether or not the desired velocity and mass are achieved depends on the integrated details of the entire ablation process including the flux and spectrum of x rays produced in the hohlraum, radiation transport to the ablation surface, and the spectral opacities of the ablator before and after blow-off, where conditions throughout may or may not be in local thermodynamic equilibrium (LTE). Since it is impossible to guarantee that all these processes can be calculated *a priori* to the accuracy necessary to achieve ignition the most practical approach is to directly measure both the velocity and mass of the ablator. These observables can then be experimentally tuned by adjusting the initial thickness of the ablator and the power in the peak of the drive to iteratively converge upon the desired conditions[5,6]. Nominally the velocity needs to be measured to $\sim \pm 2\%$ while the remaining mass needs to be measured to $\sim \pm 1.5\%$ of the initial mass. Up until now, however, it has been challenging to measure the capsule velocity and impossible to measure the ablator mass.

Streaked x-ray radiography has long been applied to ICF experiments[7] but the wealth of information encoded in this simple record has yet to be fully extracted. It is well known that the inverse Abel transform of a radiograph through a spherically-symmetric target can be used to extract the density profile, $\rho(r)$, of the capsule ablator[8,9]. Knowing this 1-D field quantity at various times ($\rho(r,t)$) then allows multiple 0-D or *average* ablator parameters to be calculated from radial moments of $\rho(r,t)$. These 0-D quantities are valuable figures-of-merit assessing the performance of an ICF implosion.

## II. AVERAGE ABLATOR QUANTITIES AS MOMENTS OF $\rho(r)$

Several important ablator quantities are defined in terms of moments of $\rho(r)$. In particular the areal density, $\langle\rho\mathrm{R}\rangle$, is given by the zeroth moment, the average radius, $\langle\mathrm{R}\rangle$, by the ratio of the first and zeroth moments, and the mass, $M$, by the second moment:

$$\langle\rho\mathrm{R}\rangle = \int^a \rho(r)\,\mathrm{d}r \tag{1}$$

$$\langle\mathrm{R}\rangle = \frac{\int^a r\rho(r)\,\mathrm{d}r}{\langle\rho\mathrm{R}\rangle} \tag{2}$$

$$M = 4\pi\int^a r^2\rho(r)\,\mathrm{d}r \tag{3}$$

$$= 4\pi\langle\rho\mathrm{R}\rangle\langle\mathrm{R}^2\rangle \tag{4}$$

where $\langle\mathrm{R}^2\rangle = \int^a r^2\rho(r)\,\mathrm{d}r/\langle\rho\mathrm{R}\rangle$. Here the lower limit of the integrals is the inner radius of the ablator (or $r = 0$ if there is no fuel) and the upper limit, $a$, is the position of the ablation front.

Rather than using $\langle\mathrm{R}\rangle$ as defined above it is often useful to define the center of mass:

$$\langle\mathrm{R}_m\rangle = \frac{\int r\rho(r)r^2\,\mathrm{d}r}{\int \rho(r)r^2\,\mathrm{d}r} \tag{5}$$

Simulations show that $\langle\mathrm{R}_m\rangle \simeq \langle\mathrm{R}\rangle$ over most of the implosion trajectory but that the time derivative of $\langle\mathrm{R}_m\rangle$ is better behaved near stagnation.

The mass can more usefully be expressed as:

$$M = 4\pi\langle\rho\mathrm{R}\rangle\left(\langle\mathrm{R}\rangle^2 + \langle\sigma^2\rangle\right) \tag{6}$$

since the variance is $\langle\sigma^2\rangle = \langle\mathrm{R}^2\rangle - \langle\mathrm{R}\rangle^2$. For the acceleration phase of an implosion it is usually true that $\langle\sigma^2\rangle \ll \langle R\rangle^2$ in which case $\langle\rho\mathrm{R}\rangle$ and $M$ are directly related, regardless of the shell thickness, for a fixed $\langle\mathrm{R}\rangle$.

Since the goal of this measurement is to determine $M(t)$ and $\langle R(t)\rangle$ (and thus the average velocity $\langle U(t)\rangle = \mathrm{d}\langle R\rangle/\mathrm{d}t$), details of $\rho(r)$ are important only insofar as they affect its first three moments. Thus fine scale structure in $\rho(r)$ is unimportant to the extent that it does not significantly affect these moments. This relaxes the requirement on spatial resolution for the diagnostic and is in part why the regularization approach described in Section IV using smoothed density profiles is successful. Determining $\rho(r,t)$ accurately is more challenging from an instrument requirement perspective than is determining its first few moments.

## III. THE INVERSE ABEL TRANSFORM METHOD AND ITS LIMITATIONS

For spherically-symmetric objects the inverse problem of tomography reduces to finding solutions of the Abel transform. In this section the well-known formulae of absorption radiography and the Abel transform are summarized and used to illustrate how the particular challenges faced in an ICF experiment make this classic problem ill-posed. This makes an explicit solution via the inverse Abel transform impossible without additional information.

For standard absorption contrast radiography the observed x-ray intensity, $I(y)$, along a measured dimension, $y$, where $y = 0$ corresponds to the center of the object with spherical symmetry, is given by:

$$I(y)/I_0(y) = \exp[-\tau(y)] \tag{7}$$

where $I_0(y)$ is the initial x-ray intensity and $\tau(y)$ is the optical depth along the line of sight.

The inverse Abel transform relates this projected optical depth to the product of the object's opacity profile at the backlighter photon energy, $\kappa_\nu(r)$, and density profile, $\rho(r)$, where both, in general, are functions of radius:

$$\kappa_\nu(r)\rho(r) = -\frac{1}{\pi}\int_r^\infty \frac{\mathrm{d}\tau(y)}{\mathrm{d}y}\frac{\mathrm{d}y}{\sqrt{y^2 - r^2}} \tag{8}$$

Thus a measurement of $\tau(y)$ allows $\rho(r)$ to be determined explicitly provided that $\kappa_\nu(r)$ is known.

In a typical streaked radiography experiment of an imploding capsule it is difficult to extract $\rho(r)$ explicitly in this fashion because there are too many unknowns. Firstly, $I_0(y)$ in Eq. 7 is unknown. For area backlighting the spatial and temporal variations in this illumination profile cannot be ignored and are difficult to measure independently. Also, for

indirectly-driven NIF capsules there is sufficient ablated plasma to further alter the effective $I_0(y)$. Secondly, a radially inhomogeneous ablator means that $\kappa_\nu(r)$ is unknown. NIF capsule designs use a graded ablator dopant which causes $\kappa_\nu(r)$ in Eq. 8 to vary throughout the implosion. An additional challenge is that implosion radiographs are particularly noisy because of photon statistics, backgrounds, and camera noise. Regardless of the numerical technique used[10] the ill-conditioned inverse Abel transform amplifies noise.

These three problems have been solved by avoiding the inverse Abel transform and using the forward Abel transform to iterate over guesses in $\rho(r)$. This allows *a priori* constraints to be applied to the form of $\rho(r)$ and $I_0(y)$ finding the optimal solution for both (Section IV) and mitigating the noise problem. For each guess in $\rho(r)$, $\kappa_\nu(r)$ can then be converted from Lagrangian space where for the unablated region it remains constant (Section V).

## IV. A REGULARIZATION APPROACH TO FINDING $\rho(r)$

### A. A priori constraints

Regularization is a technique used to solve ill-posed or ill-conditioned problems by introducing additional information as constraints[11]. These constraints reduce the number of unknowns (useful for ill-posed problems) and penalize complexity (useful for ill-conditioned problems). Such *a priori* constraints, or Bayesian priors, are most valuable when derived from specific knowledge of the problem. The simplest example of regularization is least squares curve-fitting.

Here, for the case of an implosion radiograph, the choice of constraints attempts to capture how the eye instinctively identifies the capsule limb: The capsule limb is a unique, strongly-localized feature in an otherwise smoothly-varying background. To quantify this distinction between spatial variations caused by capsule absorption and spatial variations caused by backlighter non-uniformities the following *a priori* constraints on $\rho(r)$ and $I_0(y)$ are invoked:

**A:** *That the capsule density profile has compact support.* Specifically $\rho(r) = 0$ for $r < r_{\min}$ and $r > r_{\max}$ where $r_{\min} > 0$ and $r_{\max}$ is less than the maximum radius recorded in the radiograph. Note this is not a thin shell approximation: the shell need not be thin, it just needs to be a shell. During the acceleration phase of the implosion this should be

the case. For simplicity $\rho(r)$ should also be smooth, i.e. the density profile is a bump function.

**B:** *That the backlighter intensity profile varies over a spatial scale that is larger than the shell thickness.* Experimentally this is satisfied by using a large enough backlighter laser focal spot diameter or by suitably overlapping smaller spots.

Importantly, these constraints also remove the effect of unknown attenuation by ablator blow-off. Such absorption is significant in NIF capsules because of the large amount of ablator mass removed, the presence of a mid-Z dopant, and the fact that at high implosion velocities material continues to converge immediately after ablation. As long as the scale length of this ablated material ($> 200$ $\mu$m) is larger than that of the limb ($\sim 20$ $\mu$m) the above assumptions automatically include this additional x-ray attenuation as part of the spatial variation of the backlighter. The ablated material is eliminated from the accounting by deriving an effective $I_0(y)$ appropriate for characterizing the unablated material only. Thus the fundamental distinction made between the unablated and ablated material is one of *scale length*.

The current incarnation of this regularization procedure uses curve fits to constrain the form of $\rho(r)$ and $I_0(y)$. Functional forms for $\rho(r)$ that have been tested include a rectangular profile and Gaussian profiles with various degrees of skew. For $I_0(y)$ polynomials of order 2 to 6 have been tested. As will be described below, the solution is quite insensitive to the choice of these functional forms as long as they obey the two criteria above. This suggests there exists a more generalized mathematical approach to solving this problem than the one reported here.

### B. Analysis procedure

Having set these *a priori* constraints by choosing the functional forms for $\rho(r)$ and $I_0(y)$ the following iterative procedure is used to find $\rho(r)$ at a single time step.

1. Guess the three parameters which fully describe the $\rho(r)$ bump function. For a Gaussian these correspond to the average position, the peak density, and the width.

2. For this $\rho(r)$ determine the opacity profile, $\kappa_\nu(r)$, by converting from its value in Lagrangian space at $t = 0$. This step will be described in Section V B.

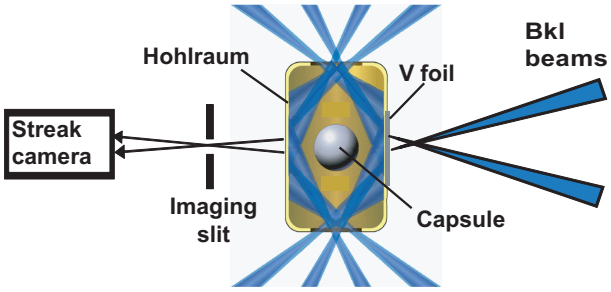


FIG. 1. Schematic (not to scale) of the OMEGA experimental setup. The Vanadium foil is glued on to the slot on the backlighter side of the hohlraum. A matching slot on the opposite side of the hohlraum allows x rays to propagate through the imaging slit to the x-ray streak camera. The imaging slit is positioned to magnify the image by a factor of 20.

3. With this $\kappa_\nu(r)\rho(r)$ profile perform the forward Abel transform to determine the optical depth, $\tau(y)$, of the object.

4. Convolve $\exp(-\tau(y))$ with the necessary instrument broadening and then recover the 'broadened' $\tau(y)$. Being able to do this is another advantage to performing the forward transform rather than its inverse.

5. Combine this instrument broadened $\tau(y)$ with the measured profile $I(y)$ to determine the effective backlighter profile using $\ln I_0(y) = \ln I(y) + \tau(y)$ (from a re-arrangement of Eq. 7).

6. Fit this effective backlighter distribution, $I_0(y)$, to a smooth profile, e.g. a polynomial of order 2, 3, or 4. Return to (1) and repeat this loop to minimize the $\chi^2$ on this fit. The result is the $\rho(r)$ which is most consistent with a smoothly varying background profile.

This procedure converges on $\rho(r)$ usually in a few iterations. The input parameters for $\rho(r)$ are then used to start the iteration afresh for next time step. In this way only one set of initial guesses need be provided to analyze an entire streaked radiograph.

## V. OPACITY OF THE UNABLATED MASS

A single radiography measurement on its own has only enough information to determine the density-opacity product, $\kappa_\nu(r)\rho(r)$, as given in Eq. 8. Finding $\rho(r)$ itself requires inde-

pendent information about $\kappa_\nu(r)$. This is a particularly important issue for capsules with a graded dopant profile[12] where the remaining opacity of the shell changes as various material layers get ablated. Here we show how $\kappa_\nu(r)$ can be determined directly from the opacity profile in Lagrangian space using the assumption that mass is ablated from outer regions of the capsule first.

### A. Validity of cold opacities

Use of cold opacities simplifies the analysis considerably since this makes $\kappa_\nu$ independent of temperature and density. LTE opacity calculations at photon energies of 6-10 keV show that in local thermodynamic equilibrium cold opacities are valid in beryllium, carbon, copper, and germanium for temperatures below 50 eV, 90 eV, 150 eV, and 300 eV respectively. These thresholds increase with density. Since temperatures in the unablated portions of the NIF capsule are expected to stay below 60 eV during the acceleration phase cold opacities are generally a good approximation.

Upon ablation opacities drop significantly due to ionization of the K-shell (in the case of beryllium and carbon) or the L-shell (in the case of copper and germanium). This provides a natural distinction between the ablated and unablated region since x-ray absorption occurs primarily in the unablated material. While this is a convenient feature for a diagnostic designed to detect only the unablated shell it is actually the scale length of the limb, as described in Section IV A, that distinguishes unablated from ablated material.

### B. Determining $\kappa_\nu(r)$ by a transformation from Lagrangian space

The heterogeneous ablator complicates the analysis since the opacity profile $\kappa_\nu(r)$ is constantly changing as material is ablated. Determining $\kappa_\nu(r)$ at each time step can still be done however by recognizing that the opacity profile for the unablated shell is time invariant in Lagrangian space. The guess for $\rho(r)$ made at the start of each iteration (Section IV B) provides the necessary transformation between Eulerian radial positions ($r$) and Lagrangian mass elements ($m$). Then, given that $\kappa_\nu(m)$ for the unablated shell is known (see previous section) and time-invariant, $\kappa_\nu(r)$ can be calculated for the assumed $\rho(r)$. Any given $\rho(r)$ is associated with a specific $\kappa_\nu(r)$ - the two are not independent. This shows the advantage

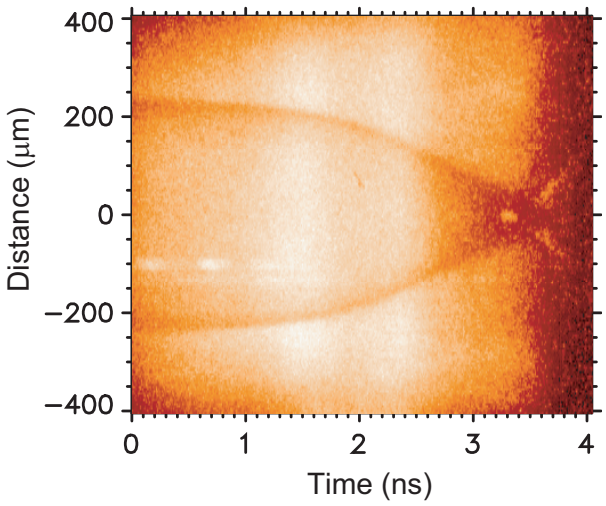


FIG. 2. A sample x-ray streak image of an imploding capsule from OMEGA showing the entire time history of the implosion from shock compression to shell acceleration to stagnation at 3.3 ns. The timing fiducials are visible at early times.

of performing the forward Abel transform and iterating about assumed forms of $\rho(r)$ rather than attempting the inverse calculation.

This technique is rigorous in that it assigns the appropriate $\kappa_\nu$ to each mass element in $\rho(r)$. An approximation that is computationally more efficient and has essentially identical results is to assume that the opacity of the remaining mass is constant across the entire density profile and equal to the average opacity of the unablated mass. This average opacity is given by

$$\overline{\kappa_\nu}(M) = \frac{\int_0^a \kappa_\nu(m)\mathrm{d}m}{\int_0^a \mathrm{d}m} = \frac{\int_0^a \kappa_\nu(r)\rho(r)r^2\mathrm{d}r}{\int_0^a \rho(r)r^2\mathrm{d}r} \tag{9}$$

This approximation works because details of the opacity distribution are higher order effects that have little effect on the first few moments of $\kappa_\nu(r)\rho(r)$.

## VI. EXPERIMENTAL TEST

### A. Experimental set-up

A scaled test of this technique was performed at the OMEGA laser facility, a neodymium-doped phosphate glass system operating with frequency-tripled, 0.35 $\mu$m light[13]. Indirectly-driven implosions were probed using area backlit x-ray streaked radiography with 5.2 keV

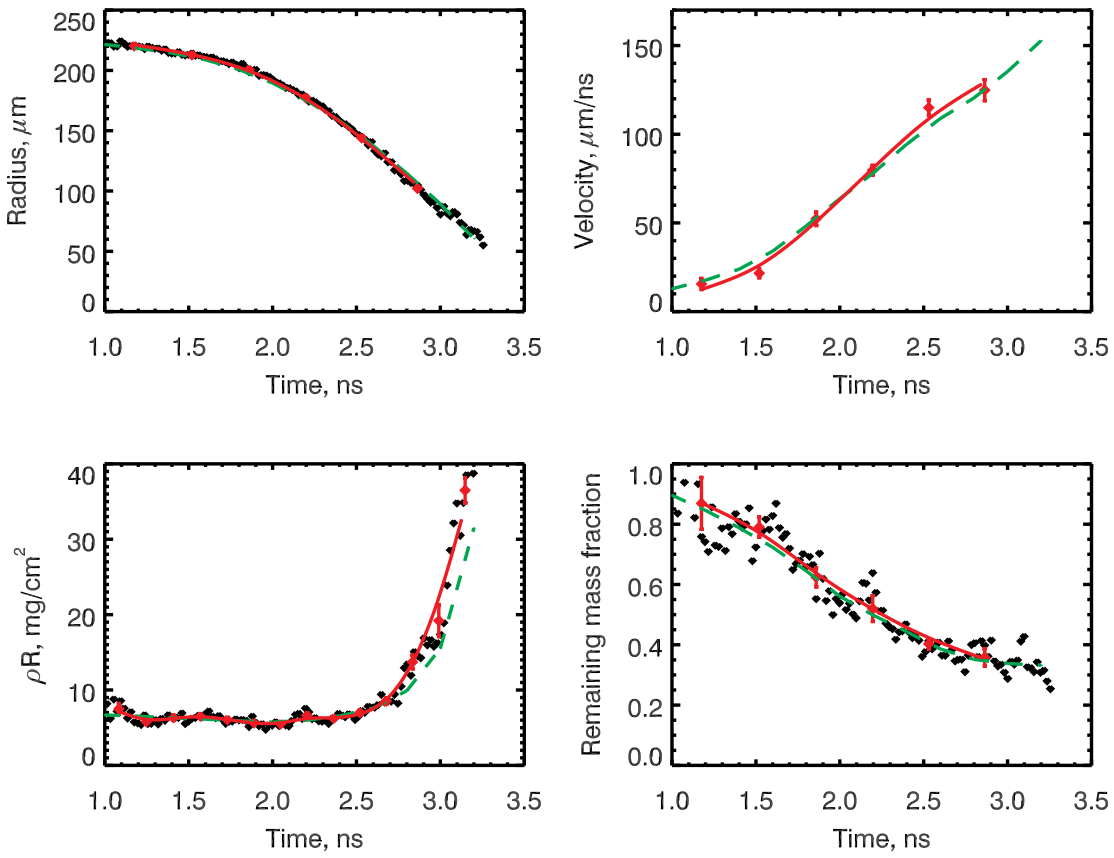


FIG. 3. Average ablator radius, velocity, $\rho$R, and remaining mass fraction versus time (black diamonds) extracted from the streak in Fig. 2. Data are binned in time allowing average values and statistical errors to be determined (red points with error bars). These points are connected by smoothing splines (solid red lines). Dashed green lines show post-shot Lasnex simulations.

x rays from Vanadium He-$\alpha$ fluorescence. A schematic of the experimental setup is shown in Fig. 1.

Copper-doped beryllium capsules with no gas fill were used. The ablators had an inner diameter of 215 $\mu$m and were composed of an inner layer of 4 $\mu$m pure Be, a 26 $\mu$m middle layer of beryllium doped with 3.0 atomic percent of Cu, and an outer layer of either 6 or 21 $\mu$m thick pure Be. Dopant concentrations were chosen so that the optical depths would be comparable to those expected when backlighting NIF capsules using higher backlighter energies.

Each capsule was held inside a hohlraum composed of 25 $\mu$m thick Au. Hohlraums were 1.6 mm in diameter and 2.5 mm long with a 1.2 mm diameter laser entrance hole (LEH) at

each end. No hohlraum gas fill was used. The axis of rotation of the hohlraum was aligned along the P6-P7 axis of the OMEGA target chamber. For radiography access two narrow slots were made on either side of the hohlraum aligned parallel to the hohlraum axis. The slot on the backlighter side (H7) was 1000 $\mu$m long and 300 $\mu$m high while that on the streak camera side (H14) was 1000 $\mu$m long and 100 $\mu$m high. The H7 slot was covered by a 5 $\mu$m thick V backlighter foil while the H14 slot was covered with a 50 $\mu$m thick CH foil to prevent closure of the slot during laser ablation of the hohlraum. Slots were offset in opposite directions from hohlraum center to account for the radiography axis (H7-H14) being 10.8° off-perpendicular from the hohlraum axis. Calibration shots were taken on hohlraums without capsules to measure the backlighter spatial profile and, in conjunction with a grid on the H14 slot, to experimentally measure the magnification.

A total of 40 beams were used to heat the hohlraum. The 20 beams illuminating each LEH were incident at 29° (5 beams), 42° (5 beams), and 59° (10 beams) to the hohlraum axis. A shaped laser pulse approximately 2.7 ns in duration was used. Due to facility constraints the same laser pulse shape was used for the backlighter pulses. Maximum available energies of $\sim$ 320 J/beam were used on all shots. Eight backlighter beams were used to illuminate the central $\sim$800 $\mu$m field of view of the hohlraum slots. Beams were tiled in space and staggered in time to optimize the x-ray emission brightness and uniformity in both space and time.

The primary diagnostic was the SSC-A x-ray streak camera[14] run with a Au photocathode. The camera sweep speed was set to capture a sweep window of $\sim$ 4 ns, giving a time resolution of $\sim$ 40 ps. A UV timing comb was used on each streak record to measure the sweep speed and provide and absolute timing reference. The multi-channel soft x-ray diagnostic Dante[15] was run to capture the time history of the hohlraum x-ray emission and thus radiation temperature.

### B. Results

X-ray streaked radiographic images were obtained on shots under similar drive conditions using targets with either 36 $\mu$m or 51 $\mu$m thick ablators. A sample streak is given in Fig. 2 for a capsule with a 36 $\mu$m thick ablator. The measured hohlraum radiation temperature reached a peak of 200 eV.

The inferred $\langle R(t)\rangle$, $\langle U(t)\rangle$, $\rho R(t)$, and $M(t)$ are shown in Fig. 3. Each black diamond represents the result from the regularization analysis at a single time step. To estimate statistical errors, data points from several adjacent time steps are grouped together into a single bin with the average and standard deviation reported in red with error bars. Average velocities are found by taking a linear fit versus time of the data points within a single bin. Also shown are the results from post-shot two-dimensional Lasnex simulations incorporating the measured laser power for each beam. These calculations are in good agreement with the data.

## VII. CONCLUSION

An x-ray streaked radiography technique to measure the time-resolved radius, velocity, $\rho$R, and mass of imploding capsules has been developed as part of the effort to achieve ignition at the NIF. $\rho(r)$ is extracted from the x-ray transmission profile at each time step with the integrated quantities - $\rho$R, radius, and mass - then being determined from the first three moments in $\rho(r)$.

Regularization is used to address the ill-posed problem of having an unknown backlighter intensity profile, $I_0(y)$. The solution is found to be that which optimally satisfies the *a priori* constraints that $\rho(r)$ is localized in radius space and $I_0(y)$ is smooth and delocalized in image space. This approach of using the different scale lengths to distinguish shell absorption variations from backlighter variations is how the human eye instinctively identifies the capsule limb in an implosion radiograph.

Tests of this technique in OMEGA experiments showed great promise. Also promising were numerical tests of this technique on simulated NIF radiographs. These will be described in a separate publication.

## VIII. ACKNOWLEDGEMENTS

We thank the OMEGA operations crew at the Laboratory for Laser Energetics for their efforts during the experiment; A. Nikroo, H. Huang, and K. Moreno at General Atomics and R. Wallace at LLNL for target fabrication; and C. W. Mauche and B. G. Wilson for the hard x-ray opacity calculations. This work was performed under the auspices of the

U.S. Department of Energy by Lawrence Livermore National Laboratory under Contract DE-AC52-07NA27344.

## REFERENCES

[1]G. H. Miller, E. I. Moses, and C. R. Wuest, Nuclear Fusion, **44**, S228 (2004).

[2]B. A. Hammel, Plasma Physics and Controlled Fusion, **48**, B497 (2006).

[3]M. Herrmann, M. Tabak, and J. Lindl, Nuclear Fusion, **41**, 99 (2001).

[4]A. Kemp, J. Meyer ter Vehn, and S. Atzeni, Phys. Rev. Lett., **86**, 3336 (2001).

[5]O. L. Landen, T. R. Boehly, D. K. Bradley, D. G. Braun, D. A. Callahan, P. M. Celliers, G. W. Collins, E. L. Dewald, L. Divol, S. H. Glenzer, A. Hamza, D. G. Hicks, N. Hoffman, N. Izumi, O. S. Jones, R. K. Kirkwood, G. A. Kyrala, P. Michel, J. Milovich, D. H. Munro, A. Nikroo, R. E. Olson, H. F. Robey, B. K. Spears, C. A. Thomas, S. V. Weber, D. C. Wilson, M. M. Marinak, L. J. Suter, B. A. Hammel, D. D. Meyerhofer, J. Atherton, J. Edwards, S. W. Haan, J. D. Lindl, B. J. MacGowan, and E. I. Moses, Phys. Plasmas, **17**, 056301 (2010).

[6]B. Spears, D. Hicks, C. Velsko, M. Stoyer, H. Robey, D. Munro, S. Haan, O. Landen, A. Nikroo, and H. Huang, Journal of Physics: Conference Series, **112**, 022003 (2008).

[7]B. A. Hammel, D. Griswold, O. L. Landen, T. S. Perry, B. A. Remington, P. L. Miller, T. A. Peyser, and J. D. Kilkenny, Physics of Fluids B: Plasma Physics, **5**, 2259 (1993).

[8]D. H. Kalantar, S. W. Haan, B. A. Hammel, C. J. Keane, O. L. Landen, and D. H. Munro, Rev. Sci. Instrum., **68**, 814 (1997).

[9]F. J. Marshall, P. W. McKenty, J. A. Delettrez, R. Epstein, J. P. Knauer, V. A. Smalyuk, J. A. Frenje, C. K. Li, R. D. Petrasso, F. H. Séguin, and R. C. Mancini, Phys. Rev. Lett., **102**, 185004 (2009).

[10]C. J. Dasch, Appl. Opt., **31**, 1146 (1992).

[11]W. H. Press, S. A. Teukolsky, W. T. Vetterling, and B. P. Flannery, *Numerical Recipes: The Art of Scientific Computing, 3rd Edition* (Cambridge University Press, New York, 2007).

[12]S. W. Haan, M. C. Herrmann, T. R. Dittrich, A. J. Fetterman, M. M. Marinak, D. H. Munro, S. M. Pollaine, J. D. Salmonson, G. L. Strobel, and L. J. Suter, Physics of Plasmas, **12**, 056316 (2005).

[13]T. R. Boehly, D. L. Brown, R. S. Craxton, R. L. Keck, J. P. Knauer, J. H. Kelly, T. J. Kessler, S. A. Kumpan, S. J. Loucks, S. A. Letzring, F. J. Marshall, R. L. McCrory, S. F. B. Morse, W. Seka, J. M. Soures, and C. P. Verdon, Optics Communications, **133**, 495 (1997).

[14]D. H. Kalantar, P. M. Bell, T. S. Perry, N. Sewall, J. Kimbrough, F. Weber, C. Diamond, and K. Piston, Rev. Sci. Instrum., **72**, 751 (2001).

[15]C. Sorce, J. Schein, F. Weber, K. Widmann, K. Campbell, E. Dewald, R. Turner, O. Landen, K. Jacoby, P. Torres, and D. Pellinen, Rev. Sci. Instrum., **77**, 10E518 (2006).